Article

Analysis of Low-Frequency 1/f Noise Characteristics for MoTe$_2$ Ambipolar Field-Effect Transistors

Bing Zhang [1,2,*]**, Congzhen Hu** [1,2]**, Youze Xin** [1,2]**, Yaoxin Li** [1,2]**, Yiyun Xie** [1,2]**, Qian Xing** [1,2]**, Zhuoqi Guo** [1,2]**, Zhongming Xue** [1,2]**, Dan Li** [1,2]**, Guohe Zhang** [1,2]**, Li Geng** [1,2]**, Zungui Ke** [3] **and Chi Wang** [4]

[1] School of Microelectronics, Xi'an Jiaotong University, Xi'an 710049, China; hucongzhen@stu.xjtu.edu.cn (C.H.); youzxin@stu.xjtu.edu.cn (Y.X.); 1143506042@stu.xjtu.edu.cn (Y.L.); 4120105068@stu.xjtu.edu.cn (Y.X.); q.xing@stu.xjtu.edu.cn (Q.X.); guozhuoqi2004@163.com (Z.G.); lincolnxzm@163.com (Z.X.); dan.li@mail.xjtu.edu.cn (D.L.); zhangguohe@mail.xjtu.edu.cn (G.Z.); gengli@xjtu.edu.cn (L.G.)
[2] Key Lab of Micro-Nano Electronics and System Integration of Xi'an City, Xi'an 710049, China
[3] Detector Laboratory of Southwest Institute of Technical Physics, Chengdu 610041, China; kezungui123@163.com
[4] ABAX Sensing Inc., Ningbo 315502, China; jxgx252584@163.com
* Correspondence: bing_zhang1982@xjtu.edu.cn

Abstract: Low-frequency electronic noise is an important parameter used for the electronic and sensing applications of transistors. Here, we performed a systematic study on the low-frequency noise mechanism for both p-channel and n-channel MoTe$_2$ field-effect transistors (FET) at different temperatures, finding that low-frequency noise for both p-type and n-type conduction in MoTe$_2$ devices come from the variable range hopping (VRH) transport process where carrier number fluctuations (CNF) occur. This process results in the broad distribution of the waiting time of the carriers between successive hops, causing the noise to increase as the temperature decreases. Moreover, we found the noise magnitude for p-type MoTe$_2$ FET hardly changed after exposure to the ambient conditions, whereas for n-FET, the magnitude increased by nearly one order. These noise characteristics may provide useful guidelines for developing high-performance electronics based on the emerging transition metal dichalcogenides.

Keywords: MoTe$_2$; low-frequency noise; carrier number fluctuations; contact resistance

1. Introduction

With the scaling of Si-based transistors approaching its limit, two-dimensional materials, as the possible building blocks of next generation electronics and optoelectronics, have attracted world-wide interest [1–4]. Although the zero-band gap of graphene greatly constrains its use in logic circuits, other 2D materials or derivatives, such as black phosphorus and transition-metal dichalcogenides (TMDs), show superior electrical and optoelectrical performance, and are considered to be promising candidates for the development of post-silicon devices [4–12]. 2H-type molybdenum ditelluride (MoTe$_2$) is a layered compound with a band gap ranging from 0.81 eV (indirect) for bulk to 1.13 eV (direct) for monolayer, enabling its excellent performance in tunneling transistors, with high tunneling current and optoelectronic devices operating from the visible to the near-infrared range [11,13–16]. Moreover, due to its ambipolar transport property and its ability to improve mobility by tuning its carrier conduction type rationally, a variety of functional electronic devices can be realized, such as complementary metal-oxide-semiconductor transistors, logic inverters, and PN junctions, which paves the way for developing MoTe$_2$-based high-performance electronics and optoelectronics [11,17–20].

Low-frequency noise usually manifests itself as slow fluctuations in the drain–source current, resulting from channel conductivity fluctuations [21–24]. It is a basic performance-limiting factor of electronic devices or circuits, in that the sensitivity and accuracy of

electronic devices, such as sensors, amplifiers, or other digital and analog electronic devices, are ultimately defined by it [25–28]. With the decrease in circuit characteristic size, low-frequency noise becomes very important to the performance of the circuit [25,29–35]. Previous reports on low-frequency noise in graphene and MoS_2 field-effect transistors suggest that the origin and mechanism of low-frequency noise is strongly dependent on the properties of the channel materials and device fabrication process [25–28,33,36–38]. To develop high-performance $MoTe_2$-based electronic devices, a thorough characterization of specific features of low-frequency noise and the methods to reduce it is required.

In this work, we investigate the low-frequency noise in $MoTe_2$ ambipolar field-effect transistors (FET). Noise measurement reveals that the noise mechanisms for both p-type and n-type conduction originate in CNF, causing the noise to increase as the temperature decreases. Subsequently, we find that large contact resistance at the metal–$MoTe_2$ interface dominates the electrical and noise characteristics of the transistors in the "on" state. Finally, we investigate the impact of ambient conditions on the noise performance of $MoTe_2$ n-FET and p-FET, finding that the noise in n-FET and p-FET changes variably following exposure to the atmospheric environment. The noise magnitude of n-FET increases by nearly one order, while in p-FET, little change is shown.

2. Materials and Methods

$MoTe_2$ thin flakes were mechanically exfoliated using the Scotch tape method and transferred onto a degenerately n-doped Si/SiO_2 (300 nm) substrate. The target $MoTe_2$ thin flakes were identified by measuring the Raman scattering spectra with a 633 nm laser under an optical microscope, and the thickness of the flakes were determined by atomic force microscopy combined with the optical contrast. Standard electron-beam lithography was employed to define the electrical contact, and a metal stack of Cr/Au (5/60 nm) was deposited by electron beam evaporation. The electrical characterization of $MoTe_2$ FET was performed in a lakeshore probe station (pressure lower than 10^{-5} Torr) using a Keithley 4200-SCS (Tektronix Inc., Beaverton, OR, USA) and a custom PDA fast probe noise measurement system.

3. Results

3.1. Basic Characteristics

A schematic image of the $MoTe_2$ field-effect transistor is shown in Figure 1a. The thickness of the flake was confirmed to be 4.9 nm by a surface line profile, as shown in Figure 1b, and the inset is an optical image of the device. Figure 1c is the Raman spectrum collected from the position indicated in Figure 1b. The peaks at around 171, 234, and 289 cm^{-1} can be attributed to the A_{1g}, E^1_{2g}, and B^1_{2g} vibration modes, respectively, which is consistent with previous reports [13–15]. The room-temperature transfer characteristics of the device under different bias voltages are shown in Figure 1d. The increase in the drain current I_{ds} with increasing gate voltage for both negative and positive polarities demonstrates the ambipolar operation of the $MoTe_2$ FET, and the obvious saturation trend of the drain current at positive gate voltage (~7.5 V) can be a result of the contact resistance at the metal–$MoTe_2$ interface [39]. The on/off ratio at V_{ds} = 1.0 V is found to be ~7.1 × 10^3 for $MoTe_2$ p-FET, and ~1.5 × 10^4 for $MoTe_2$ n-FET, respectively. Field-effect mobility can be extracted from the equation:

$$\mu_{FE} = \frac{1}{C_{ox}} \frac{1}{V_{ds}} \frac{L}{W} \frac{dI_{ds}}{dV_{bg}} \tag{1}$$

In this equation, L and W are the length and width of the channel, respectively. C_{ox} is the gate oxide capacitance per unit area, and V_{ds} is the source–drain bias voltage. The linear fitting was taken at the linear region of the transfer characteristics, and a mobility of 2.66 cm^2/Vs for hole and 2.03 cm^2/Vs for electron can be extracted, respectively. Figure 1e,f reveal the output characteristics of the $MoTe_2$ FET with a bias voltage ranging from −3 to 0 V for p-FET, and 0–3 V for n-FET at different gate voltages. The good linear shape at small bias voltage and the obvious saturation of the current for p-FET imply that the contact

between MoTe$_2$ and metal electrode is ohmic or the contact resistance is comparably small. However, for n-FET, the drain current increases nonlinearly with bias voltage, indicating the existence of significant contact resistance at the metal–MoTe$_2$ interface, which will suppress the electron injection from the metal electrode into the conducting channel and may cause series resistance noise [40].
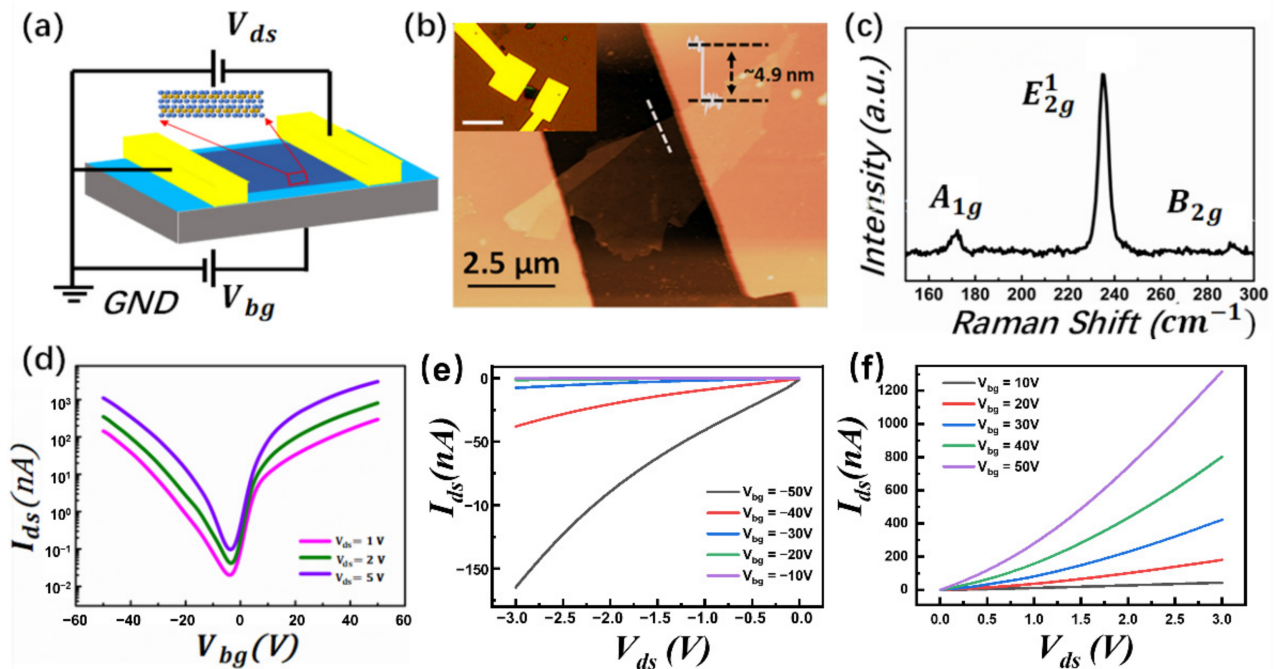

Figure 1. (**a**) Schematic image of MoTe$_2$ transistor. (**b**) Atomic force microscope image of the transistor. The inset is the optical image of the transistor, scale bar is 5µm. (**c**) Raman spectrum of the MoTe$_2$ measured under 633 nm laser flake in (**b**). (**d**) Transfer curves of the MoTe$_2$ transistor with the back gate voltage sweeping from −50 to 50 V at a step of 0.8 V at different bias voltage: V_{ds} = 1.0 V, 2.0 V, and 5.0 V, respectively. (**e**) Output curves of the transistor with bias voltage swept from −3.0 V to 0 V under different back gate voltages ranging from −50 to −10 V at a step of 10 V. (**f**) Output curves of the transistor with bias voltage swept from 0 to 3 V under different back gate voltages ranging from 10 to 50 V at a step of 10 V.

3.2. Noise Characteristics

The noise characterization of MoTe$_2$ FET is shown in Figure 2. The noise power spectral density S_I of the MoTe$_2$ p-FET at four different gate voltages between 1 Hz to 100 kHz with a bias voltage kept at V_{ds} = 2.5 V is shown in Figure 2a. When the p-FET is in the "on" state, the noise spectra follow the typical 1/f dependence and can be quantitatively characterized by

$$S_I = A I_{ds}^2 / f^\beta \tag{2}$$

In this equation, S_I is the current noise power spectral density, A is the noise amplitude, I_{ds} is the current through the device channel, f is the frequency, and β is the frequency exponent. However, when the gate voltage is close to the flat band voltage, or the device is in the "off" state, the noise spectra at a high frequency increase and deviate from 1/f dependence because of the instrumental noise floor. Figure 2b shows the noise characteristics of the MoTe$_2$ n-FET in the same device and similar behavior can be observed.
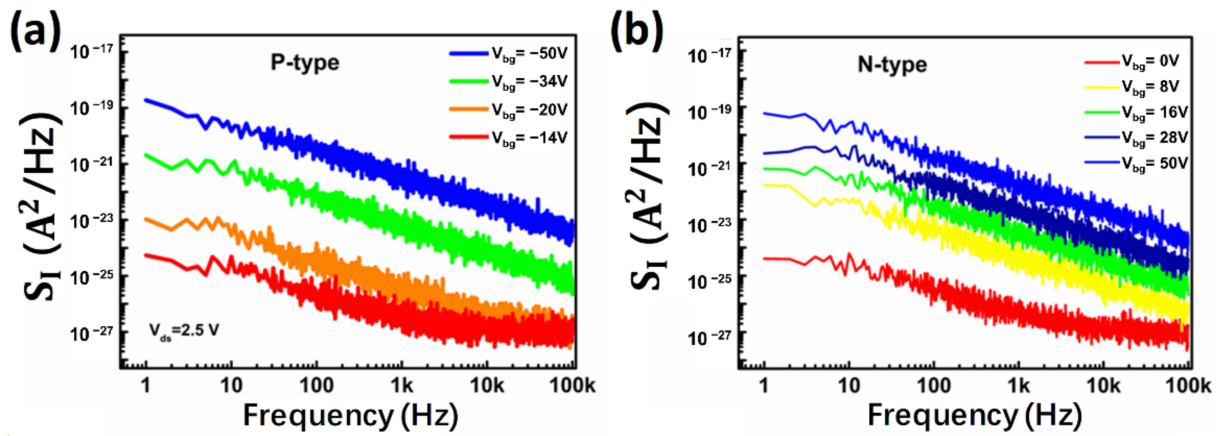
Figure 2. (**a**) Noise power spectral density S_I as a function of frequency at different gate voltages for MoTe$_2$ p-FET. (**b**) Noise power spectral density S_I as a function of frequency at different gate voltages for MoTe$_2$ n-FET.

The extracted frequency exponent β as a function of V_{bg} was extracted from a least-square fit of Figure 2a using Equation (2), which ranges from 0.95 to 1.1 in the "on" state as shown in Figure 3a. To determine whether the metal–MoTe$_2$ contact barrier contributes to the noise of the MoTe$_2$ FET, the normalized noise power spectra S_I/I_{ds}^2 of both p-FET ($V_{bg} = -50$ V) and n-FET ($V_{bg} = 46$ V), as a function of frequency at different bias voltages, were performed, as shown in Figure 3b. It was found that the normalized noise power spectra S_I/I_{ds}^2 for p-FET are independent of the bias voltage, indicating that the noise mainly originated from the MoTe$_2$ conducting channel itself. However, for n-FET, the normalized noise power spectra S_I/I_{ds}^2 are strongly dependent on bias voltage, suggesting the contact barrier is one of the main contributors to the noise of n-FET. These results are consistent with initial DC characterization results that significant contact resistance exists at the metal–MoTe$_2$ interface.
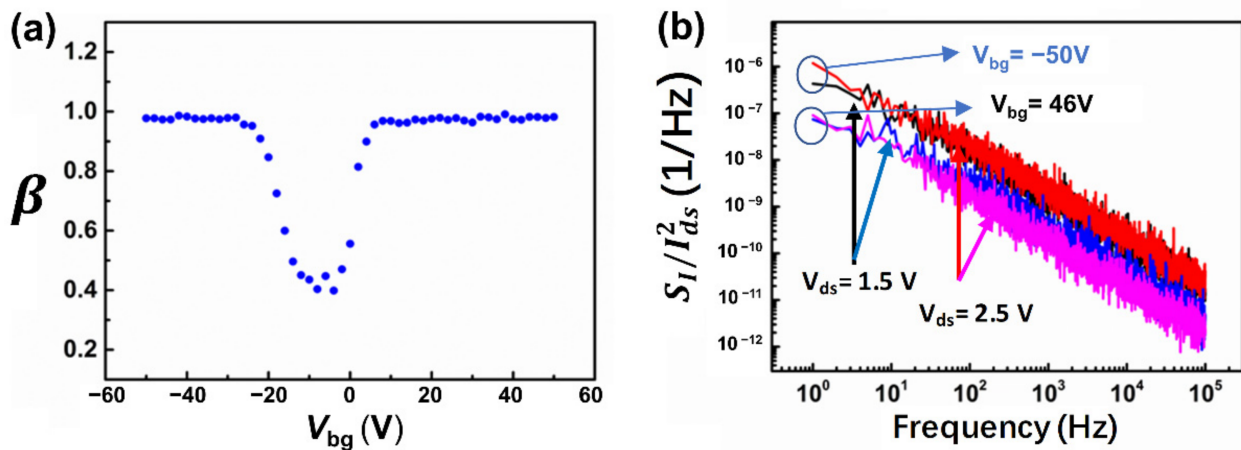

Figure 3. (**a**) Frequency exponent β as a function of gate voltage. (**b**) Normalized noise spectra S_I/I_{ds}^2 as a function of frequency at different bias voltage: $V_{ds} = 1.5$ V, 2.5 V under different gate voltage: $V_{bg} = -50$ V, 46 V.

There are two models to describe the noise mechanism of the conventional FET: the carrier number fluctuation (CNF) model, which can be expressed by:

$$S_I/I_{ds}^2 = (g_m/I_{ds})2S_{Vfb} \tag{3}$$

$$S_{Vfb} = q^2 K_B T N_{it}/WLC_{ox}^2 f \tag{4}$$

where S_{vfb} is the flat-band voltage spectral density and q is the elementary charge, K_B is the Boltzmann constant, T is the absolute temperature, N_{it} is the effective trap density, and C_{ox} is the gate unit capacitance, respectively. The other model is the Hooge mobility fluctuation (HMF) model which is expressed by

$$S_I/I_{ds}^2 = q\alpha_H\mu_{eff}V_{ds}/fL^2I_{ds} \tag{5}$$

where the Hooge parameter α_H is an empirical dimensionless constant. If the series resistance contributes to the low-frequency noise, the total current noise changes into the form

$$S_I/I_{ds}^2 = \left(S_I/I_{ds}^2\right)_{channel} + (I_{ds}/V_{ds})^2 S_{Rsd} \tag{6}$$

where S_{Rsd} is the spectral density of series resistance [22,23]. From the equation, we can see that if the normalized drain current noise increases at a high current, it can be indicative of an enhanced low-frequency noise contribution of the series resistance.

To uncover the noise mechanism of this few-layer MoTe$_2$-based transistor, S_I/I_{ds}^2 at f = 100 Hz and its corresponding $(g_m/I_{ds})^2$ at 300 K as a function of the drain current for the MoTe$_2$ p-FET and n-FET are plotted in Figure 4a,b, respectively. From Figure 4a, we can observe that S_I/I_{ds}^2 and its corresponding $(g_m/I_{ds})^2$ follow the same trend over a wide drain current range, indicating that the low-frequency noise in MoTe$_2$ p-FET comes from the carrier number fluctuation [24]. However, for n-FET, as shown in Figure 4b, we found that S_I/I_{ds}^2 and its corresponding $(g_m/I_{ds})^2$ follow the same trend. At small currents larger than 2.0×10^{-7} A, the normalized noise power spectra S_I/I_{ds}^2 deviate from their corresponding $(g_m/I_{ds})^2$ and start to increase alongside the drain current. Therefore, when the drain current is $I_{ds} < 2.0 \times 10^{-7}$ A, noise is from the carrier number fluctuation, while when the drain current is $I_{ds} > 2.0 \times 10^{-7}$ A, the noise of the n-FET mainly comes from the metal–MoTe$_2$ contact barrier, which is consistent with results shown in Figure 3b.
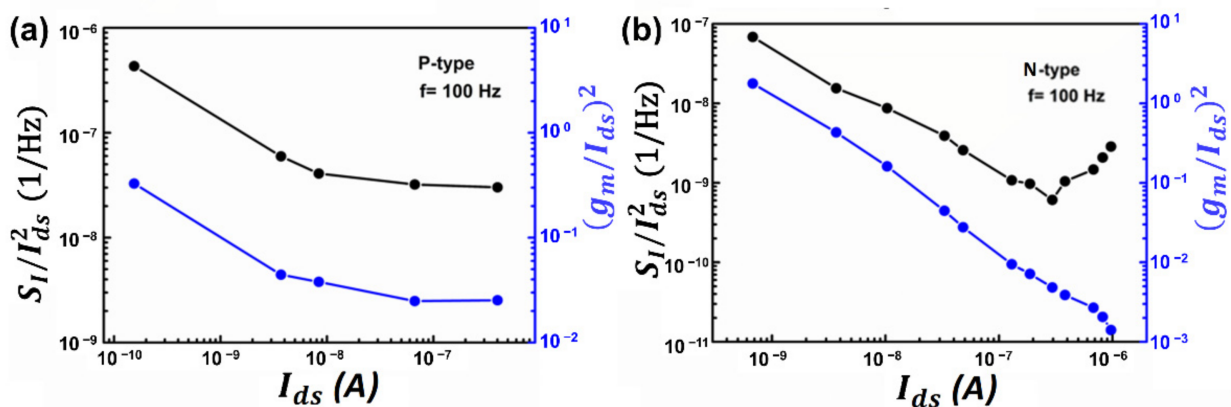

Figure 4. (**a**) S_I/I_{ds}^2 and its corresponding $(g_m/I_{ds})^2$ as a function of drain current for MoTe$_2$ p-FET. (**b**) S_I/I_{ds}^2 and its corresponding $(g_m/I_{ds})^2$ as a function of drain current for MoTe$_2$ n-FET.

To further investigate the noise mechanisms, we characterized the transfer characteristics of the device (Figure 5), and normalized the noise power spectra S_I/I_{ds}^2 as a function of gate voltage (Figure 6a for p-FET and Figure 6b for n-FET, respectively) at different temperatures from 100 to 300 K. At different temperatures, S_I/I_{ds}^2 almost follows the same trend for both p-FET and n-FET, indicating that the noise mechanism is independent of temperature. Moreover, we observed that the magnitude of normalized noise spectra S_I/I_{ds}^2 for both MoTe$_2$ p-FET and n-FET decreases as temperatures increase, which is inconsistent with previous reports which suggest that the magnitude of noise amplitude decreases alongside the temperature when dominated by a thermally activated process [32]. Previous theoretical studies reported that the variable range hopping (VRH) transport in transistors

will result in the broad distribution of the waiting time of the carriers between successive hops, causing the noise to increase as the temperature decreases [41,42].
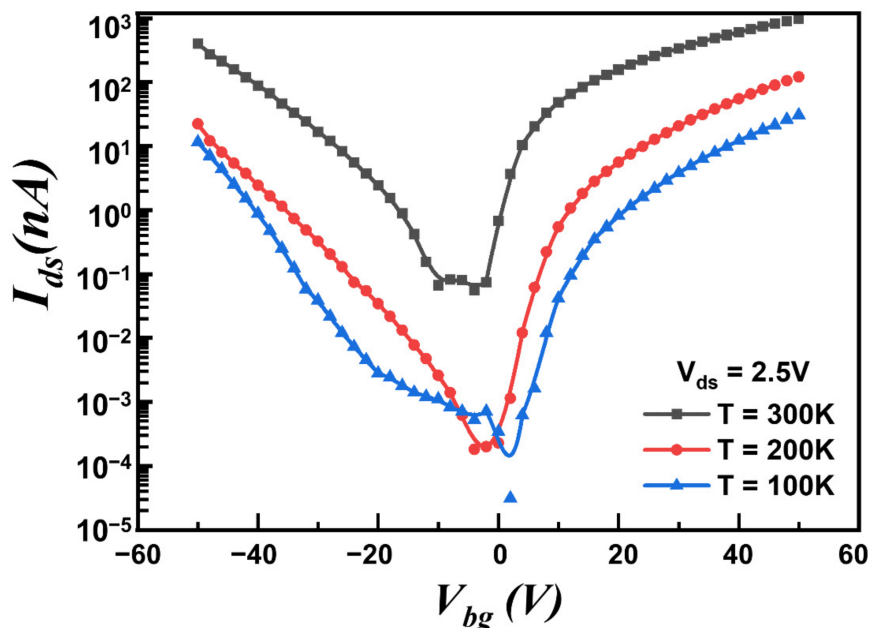

Figure 5. Transfer curves of the MoTe$_2$ transistor at different temperatures from 100 to 300 K at a step of 100 K.
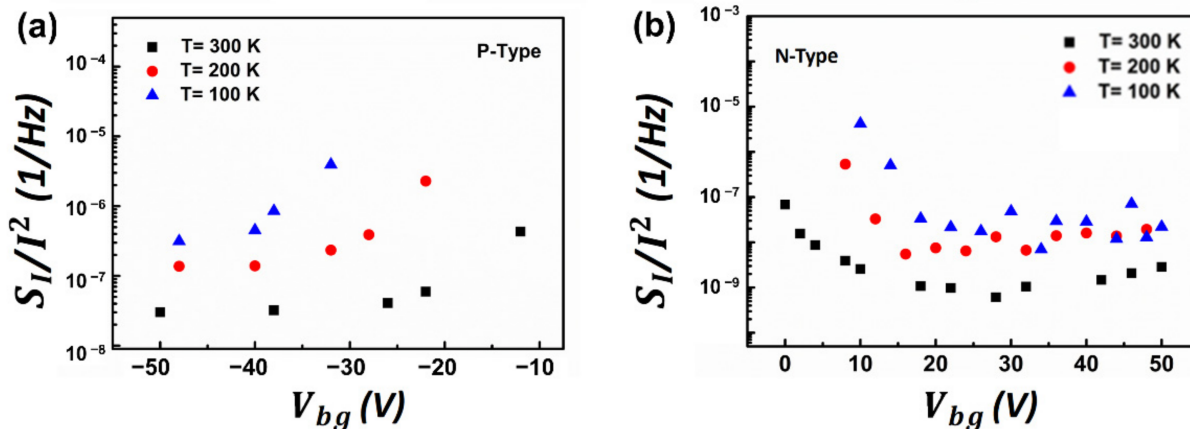

Figure 6. (**a**) S_I / I_{ds}^2 as function of gate voltage for p-FET and (**b**) for n-FET at different temperature from 100 to 300 K.

To experimentally validate the theoretical predictions, and demonstrate whether this phenomenon is occasional, several MoTe$_2$ devices with a channel thickness ranging from 4.9 nm to 12 nm were fabricated and studied experimentally. The noise characteristics were electrically measured at different temperatures. All these experiments show the same pattern around noise characteristics. Experimental results of MoTe$_2$ devices with a channel thickness of 8.0 nm are shown in Figure 7a,b. The same decreasing behavior of S_I / I_{ds}^2 with increasing temperatures was also observed. Therefore, conductivity (σ) of two terminals as a function of temperature was characterized to determine the conduction mechanism within the MoTe$_2$ channel, as shown in Figure 7c. We found that the variation of σ with T in MoTe$_2$ transistors can be modeled well with the variable I_{ds} hopping (VRH) transport.

$$\sigma = AT^{-0.8} exp\left[(T_0/T)^{1/3} \right] \tag{7}$$

$$N = (V_{bg} - V_{th})LWC_{ox}/q \tag{8}$$

where V_{th} is the threshold voltage of the device, is the total number of carriers in the conducting channel, before and after the exposures were shown in Figure 8b for p-FET and Figure 8c for n-FET, respectively. As demonstrated, for n-FET, the magnitude of noise changes increases nearly by one order, while for p-FET, it shows no apparent change, which agrees with previous studies [25,43–45]. For n-FET, adsorbates from ambient conditions function as trapping centers, trapping and scattering the electron within the channel, while for p-FET, the concentration of carriers will increase because of the ambient doping; thus, conductance increases and noise, in comparison, either decreases or hardly changes.
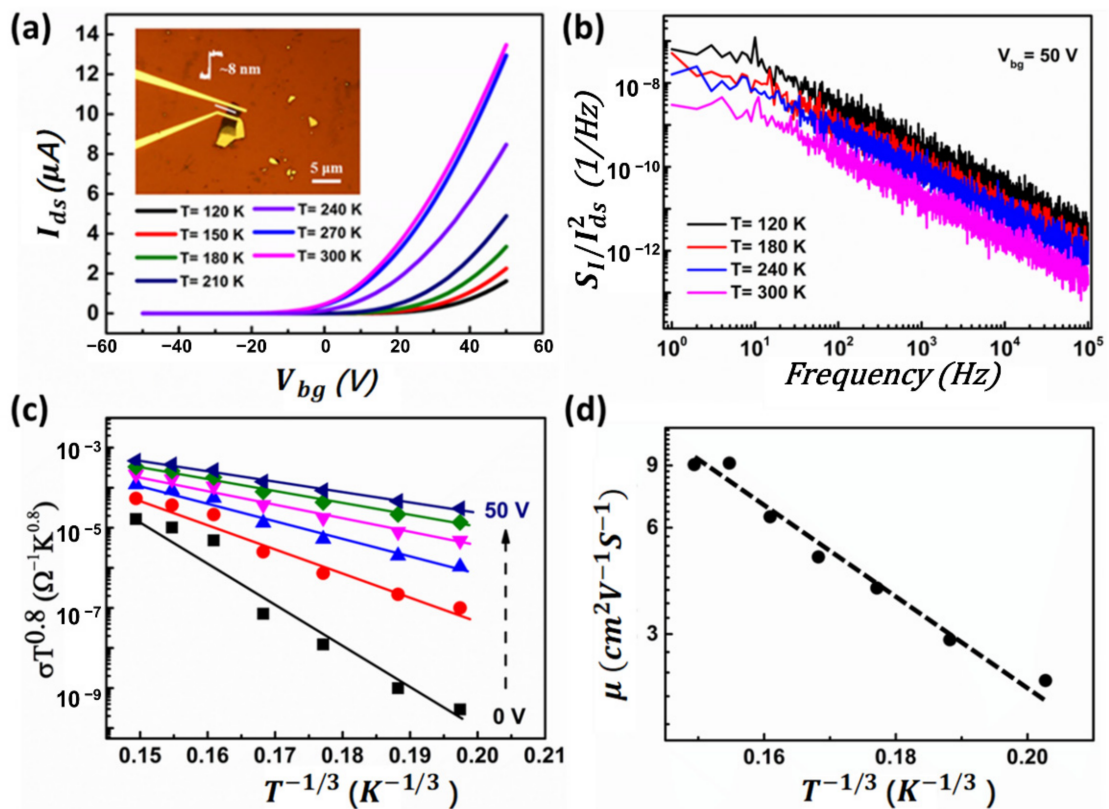

Figure 7. Conduction mechanism in an MoTe$_2$ transistor. (**a**) Transfer curves of MoTe$_2$ FET at different temperatures from 120 to 300 K at a step of 30 K. (**b**) Normalized noise spectra S_I/I_{ds}^2 as a function of frequency at different temperatures from 120 s to 300 K at a step of 60 K. (**c**) Conductivity σ as a function of temperature at different gate voltages ranging from 0 to 50 V at a step of 10 V. (**d**) Field-effect mobility of the MoTe$_2$ transistor as a function of temperature.
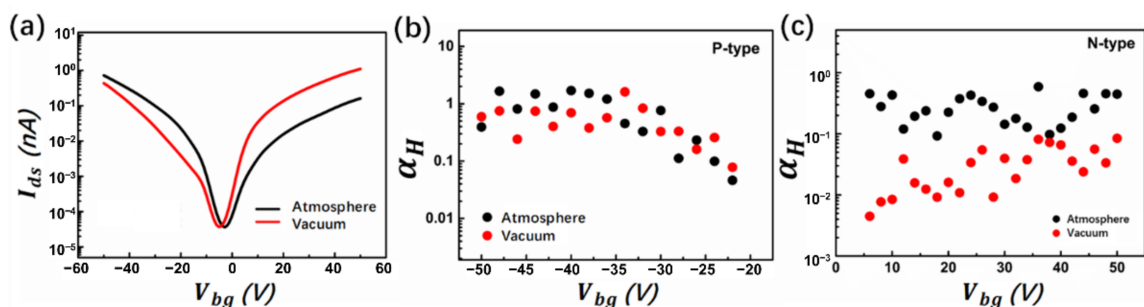

Figure 8. Impact of ambient conditions on the noise of MoTe$_2$ transistor. (**a**) Transfer curves of MoTe$_2$ FET before and after exposure to ambient conditions. (**b**) Hooge parameter α_H as a function of gate voltage before and after exposure to ambient conditions for MoTe$_2$ p-FET and (**c**) for MoTe$_2$ n-FET.

4. Conclusions

In conclusion, we characterized the noise features in MoTe$_2$ few-layered ambipolar transistors. The noise mechanism of the MoTe$_2$ p-FET and n-FET was characterized as carrier number fluctuations, which were caused by variable range hopping transport rather than thermally activated transport in the MoTe$_2$ conducting channel, and stayed the same with temperature. The noise of n-channel and p-channel of MoTe$_2$ ambipolar transistors showed a different response upon exposure to ambient conditions, which indicates that n-channel transport is more sensitive to ambient conditions. These noise characteristics may provide useful guidelines to develop high-performance electronics based on the emerging transition metal dichalcogenides and can be a useful diagnostic tool to identify the conduction mechanism.

Author Contributions: Conceptualization and methodology, B.Z.; hardware, Y.X. (Youze Xin); validation, C.H., Y.L. and Y.X. (Yiyun Xie); formal analysis, Z.G. and Z.X.; investigation, B.Z.; data curation, Z.K.; writing—original draft preparation, Q.X.; writing—review and editing, C.W.; visualization, C.W.; supervision, G.Z.; project administration, L.G.; funding acquisition, B.Z. and D.L. All authors have read and agreed to the published version of the manuscript.

Institutional Review Board Statement: Not applicable.

Informed Consent Statement: Not applicable.

Data Availability Statement: Not applicable.

Conflicts of Interest: The authors declare no conflict of interest.

References

1. Fiori, G.; Bonaccorso, F.; Iannaccone, G.; Palacios, T.; Neumaier, D.; Seabaugh, A.; Sanjay, K.; Colombo, L. Electronics based on two-dimensional materials. *Nat. Nanotechnol.* **2014**, *9*, 768. [CrossRef] [PubMed]
2. Geim, A.K.; Novoselov, K.S. The structure of suspended graphene sheets. *Nat. Mater.* **2007**, *6*, 183. [CrossRef] [PubMed]
3. Novoselov, K.S.; Jiang, D.; Schedin, F.; Booth, T.J.; Khotkevich, V.V.; Morozov, S.V.; Geim, A.K. Electric Field Effect in Atomically Thin Carbon Films. *Proc. Natl. Acad. Sci. USA* **2005**, *102*, 10451. [CrossRef] [PubMed]
4. Radisavljevic, B.; Radenovic, A.; Brivio, J.; Giacometti, I.V.; Kis, A. Single-layer MoS$_2$ transistors. *Nat. Nanotechnol.* **2011**, *6*, 147. [CrossRef] [PubMed]
5. Yoon, J.; Park, W.; Bae, G.Y.; Kim, Y.; Jang, H.S.; Hyun, Y.; Lim, S.K.; Kahng, Y.H.; Hong, W.K.; Lee, B.H. Highly Flexible and Transparent Multilayer MoS$_2$ Transistors with Graphene Electrodes. *Small* **2013**, *9*, 3295. [CrossRef]
6. Ye, L.; Li, H.; Chen, Z.; Xu, J. Robust and stretchable indium gallium zinc oxide-based electronic textiles formed by cilia-assisted transfer printing. *ACS Photonics* **2016**, *3*, 692. [CrossRef]
7. Das, S.; Robinson, J.A.; Dubey, M.; Terrones, H.; Terrones, M. Beyond Graphene: Progress in Novel Two-Dimensional Materials and van der Waals Solids. *Annu. Rev. Mater. Res.* **2015**, *45*, 1–27. [CrossRef]
8. Li, L.; Yu, Y.; Ye, G.J.; Ge, Q.; Ou, X.; Wu, H.; Feng, D.L.; Chen, X.H.; Zhang, Y.B. Black phosphorus field-effect transistors. *Nat. Nanotechnol.* **2014**, *9*, 372. [CrossRef]
9. Zhang, Y.J.; Ye, J.T.; Yomogida, Y.; Takenobu, T.; Iwasa, Y. Formation of a Stable p-n Junction in a Liquid-Gated MoS$_2$ Ambipolar Transistor. *Nano Lett.* **2013**, *13*, 3023. [CrossRef]
10. Yu, L.L.; Zubair, A.; Santos, E.J.G.; Zhang, X.; Lin, Y.X.; Zhang, Y.H.; Palacios, T. Transport Properties of a MoS$_2$/WSe$_2$ Heterojunction Transistor and its Potential for Application. *Nano Lett.* **2015**, *15*, 4928. [CrossRef]
11. Lin, Y.L.; Xu, Y.; Wang, S.T.; Li, S.L.; Mahito, Y.; Alex, A.F.; Li, W.W.; Sun, H.B.; Shu, N.; Jian, W.B.; et al. Barrier inhomogeneities at vertically stacked graphene-based heterostructures. *Adv. Mater.* **2014**, *26*, 3263. [CrossRef]
12. Koppens, F.H.; Mueller, T.; Avouris, P.; Ferrari, A.C.; Vitiello, M.S.; Polini, M. Photodetectors based on graphene, other two-dimensional materials and hybrid systems. *Nat. Nanotechnol.* **2014**, *9*, 780. [CrossRef]
13. Pradhan, N.R.; Rhodes, D.; Feng, S.; Yan, X.; Balicas, L. Field-Effect Transistors Based on Few-Layered α-MoTe$_2$. *ACS Nano* **2014**, *8*, 6. [CrossRef] [PubMed]
14. Ruppert, C.; Aslan, O.B.; Heinz, T.F. Optical Properties and Band Gap of Single- and Few-Layer MoTe$_2$ Crystals. *Nano Lett.* **2014**, *14*, 6231. [CrossRef] [PubMed]
15. Fathipour, S.; Ma, N.; Hwang, W.S.; Protasenko, V.; Seabaugh, A. Exfoliated multilayer MoTe$_2$ field-effect transistors. *Appl. Phys. Lett.* **2014**, *105*, 192101. [CrossRef]

16. Chen, J.; Feng, Z.; Fan, S.; Shi, S.; Yue, Y.; Shen, W.; Xie, Y.; Wu, E.; Sun, C.; Liu, J. Contact Engineering of Molybdenum Ditelluride Field Effect Transistors through Rapid Thermal Annealing. *ACS Appl. Mater.* **2017**, *9*, 30107. [CrossRef]

17. Qu, D.; Liu, X.; Ming, H.; Lee, C.; Yoo, W.J. Carrier-Type Modulation and Mobility Improvement of Thin $MoTe_2$. *Adv. Mater.* **2017**, *29*, 1606433. [CrossRef]

18. Larentis, S.; Fallahazad, B.; Movva, H.; Kim, K.; Rai, A.; Taniguchi, T.; Watanabe, K.; Banerjee, S.K.; Tutuc, E. Reconfigurable Complementary Monolayer $MoTe_2$ Field-Effect Transistors for Integrated Circuits. *ACS Nano* **2017**, *11*, 4832. [CrossRef] [PubMed]

19. Feng, Z.; Xie, Y.; Chen, J.; Yu, Y.; Zheng, S.; Zhang, R.; Li, Q.; Chen, X.; Sun, C.; Zhang, H. Highly sensitive $MoTe_2$ chemical sensor with fast recovery rate through gate biasing. *2D Mater.* **2017**, *4*, 025018. [CrossRef]

20. Huang, H.; Wang, J.; Hu, W.; Liao, L.; Wang, P.; Wang, X.; Fan, G.; Chen, Y.; Wu, G.; Luo, W.; et al. Highly sensitive visible to infrared $MoTe_2$ photodetectors enhanced by the photogating effect. *Nat. Nanotechnol.* **2016**, *27*, 445201. [CrossRef] [PubMed]

21. Pal, A.N.; Ghatak, S.; Kochat, V.; Sneha, E.S.; Ghosh, A. Microscopic Mechanism of 1/f Noise in Graphene: Role of Energy Band Dispersion. *ACS Nano* **2011**, *5*, 2075. [CrossRef] [PubMed]

22. Ghibaudo, G. Ultimately Thin Double-Gate SOI MOSFETs. *SPIE* **2003**, *5113*, 13.

23. Hooge, F.N. 1/f noise sources. *IEEE Trans. Electron Devices* **1994**, *41*, 1926. [CrossRef]

24. Lin, Y.F.; Xu, Y.; Suen, Y.W.; Yamamoto, M.; Nakaharai, S.; Ueno, K.; Tsukagoshi, K. Origin of Noise in Layered $MoTe_2$ Transistors and its Possible Use for Environmental Sensors. *Adv. Mater.* **2015**, *27*, 6612. [CrossRef] [PubMed]

25. Sangwan, V.K.; Arnold, H.N.; Jariwala, D.; Marks, T.J.; Lauhon, L.J.; Hersam, M.C. Low-Frequency Electronic Noise in Single-Layer MoS_2 Transistors. *Nano Lett.* **2013**, *13*, 4351. [CrossRef]

26. Cheng, Z.; Li, Q.; Li, Z.; Zhou, Q.; Fang, Y. Suspended Graphene Sensors with Improved Signal and Reduced Noise. *Nano Lett.* **2010**, *10*, 1864. [CrossRef]

27. Renteria, J.; Samnakay, R.; Rumyantsev, S.L.; Jiang, C.; Goli, P.; Shur, M.S.; Balandin, A.A. Low-frequency 1/f noise in MoS_2 transistors: Relative contributions of the channel and contacts. *Appl. Phys. Lett.* **2014**, *104*, 153104. [CrossRef]

28. Rumyantsev, S.; Liu, G.; Stillman, W.; Shur, M.; Balandin, A.A. Electrical and noise characteristics of graphene field-effect transistors: Ambient effects, noise sources and physical mechanisms. *J. Phys.* **2010**, *22*, 395302. [CrossRef]

29. Pellegrini, B. 1/f noise in graphene. *Eur. Phys. J. B* **2013**, *86*, 373. [CrossRef]

30. Kumar, C.; Kuiri, M.; Jung, J.; Das, T.; Das, A. Tunability of 1/f Noise at Multiple Dirac Cones in hBN Encapsulated Graphene Devices. *Nano Lett.* **2016**, *6*, 1042.

31. Levinshtein, M.E.; Pascal, F.; Contreras, S.; Knap, W.; Rumyantsev, S.L.; Gaska, R.; Yang, J.W.; Shur, M.S. AlGaN/GaN high electron mobility field effect transistors with low 1/f noise. *Appl. Phys. Lett.* **1998**, *72*, 3053. [CrossRef]

32. Li, X.F.; Du, Y.C.; Si, M.W.; Yang, L.M.; Li, S.C.; Li, T.Y.; Xiong, X.; Ye, P.D.; Wu, Y.Q. Three-layer phosphorene-metal interfaces. *Nanoscale* **2016**, *8*, 3572. [CrossRef] [PubMed]

33. Xie, X.X.; Sarkar, D.; Liu, W.; Kang, J.; Banerjee, K. A subthermionic tunnel field-effect transistor with an atomically thin channel. *ACS Nano* **2014**, *8*, 5633. [CrossRef]

34. Ji, H.; Joo, M.K.; Yun, Y.; Park, J.H.; Lee, G.; Moon, B.H.; Yi, H.; Suh, D.; Lim, S.C. Suppression of Interfacial Current Fluctuation in $MoTe_2$ Transistors with Different Dielectrics. *ACS Appl. Mater. Interfaces* **2016**, *8*, 19082. [CrossRef] [PubMed]

35. Balandin, A.A. Two-dimensional phonon transport in graphene. *Nat. Nanotechnol.* **2013**, *8*, 549. [CrossRef] [PubMed]

36. Kochat, V.; Tiwary, C.S.; Biswas, T.; Ramalingam, G.; Hsieh, K.; Chattopadhyay, K.; Raghavan, S.; Jain, M.; Ghosh, A. Magnitude and Origin of Electrical Noise at Individual Grain Boundaries in Graphene. *Nano Lett.* **2016**, *16*, 562. [CrossRef]

37. Lin, Y.M.; Avouris, P. Electrical transport and 1/f noise in semiconducting carbon nanotubes. *Nano Lett.* **2008**, *8*, 2119. [CrossRef]

38. Kim, J.K.; Song, Y.; Kim, T.Y.; Cho, K.; Pak, J.; Choi, Y.B.; Shin, J.; Chung, S.; Lee, T. Protective effects of triple fermented barley extract (FBe) on indomethacin-induced gastric mucosal damage in rats. *Nat. Nanotechnol.* **2017**, *28*, 47LT01. [CrossRef]

39. Yan, S.L.; Xie, Z.J.; Chen, J.H.; Taniguchi, T.; Watanabe, K. Electrically Tunable Energy Bandgap in Dual-Gated Ultra-Thin Black Phosphorus Field Effect Transistors. *Chin. Phys. B* **2017**, *34*, 047304. [CrossRef]

40. Delker, C.J.; Zi, Y.; Yang, C.; Janes, D.B. Current and Noise Properties of InAs Nanowire Transistors with Asymmetric Contacts Induced by Gate Overlap. *IEEE Trans. Electron Devices* **2013**, *60*, 2900. [CrossRef]

41. Shklovskii, B. Dimensional quantization in a-Si:H quantum-well structures: The alloy model. *Phys. Rev. B* **2003**, *67*, 045201. [CrossRef]

42. Qiu, H.; Xu, T.; Wang, Z.L.; Ren, W.; Nan, H.Y.; Ni, Z.H.; Chen, Q.; Yuan, S.J.; Miao, F.; Song, F.Q.; et al. Modulating the properties of MoS2 by plasma thinning and defect engineering. *Nat. Commun.* **2013**, *4*, 2642. [CrossRef] [PubMed]

43. Ghatak, S.; Pal, A.N.; Ghosh, A. Nature of Electronic States in Atomically Thin MoS_2 Field-Effect Transistors. *ACS Nano* **2011**, *5*, 7707. [CrossRef] [PubMed]

44. Ishigami, M.; Chen, J.H.; Williams, E.D.; Tobias, D.; Chen, T.F.; Fuhrer, M.S. Hooge's constant for carbon nanotube field effect transistors. *Appl. Phys. Lett.* **2006**, *88*, 203116. [CrossRef]

45. Deen, M.J.; Marinov, O.; Holdcroft, S.; Woods, W. Low-frequency noise in polymer transistors. *IEEE Trans. Electron Devices* **2001**, *48*, 1688. [CrossRef]